Supplement of The Cryosphere, 19, 3193–3225, 2025
https://doi.org/10.5194/tc-19-3193-2025-supplement

The Cryosphere Open Access EGU

Supplement of

Wind and topography underlie correlation between seasonal snowpack, mountain glaciers, and late-summer streamflow

Elijah N. Boardman et al.

Correspondence to: Elijah N. Boardman (eli.boardman@mountainhydrology.com)

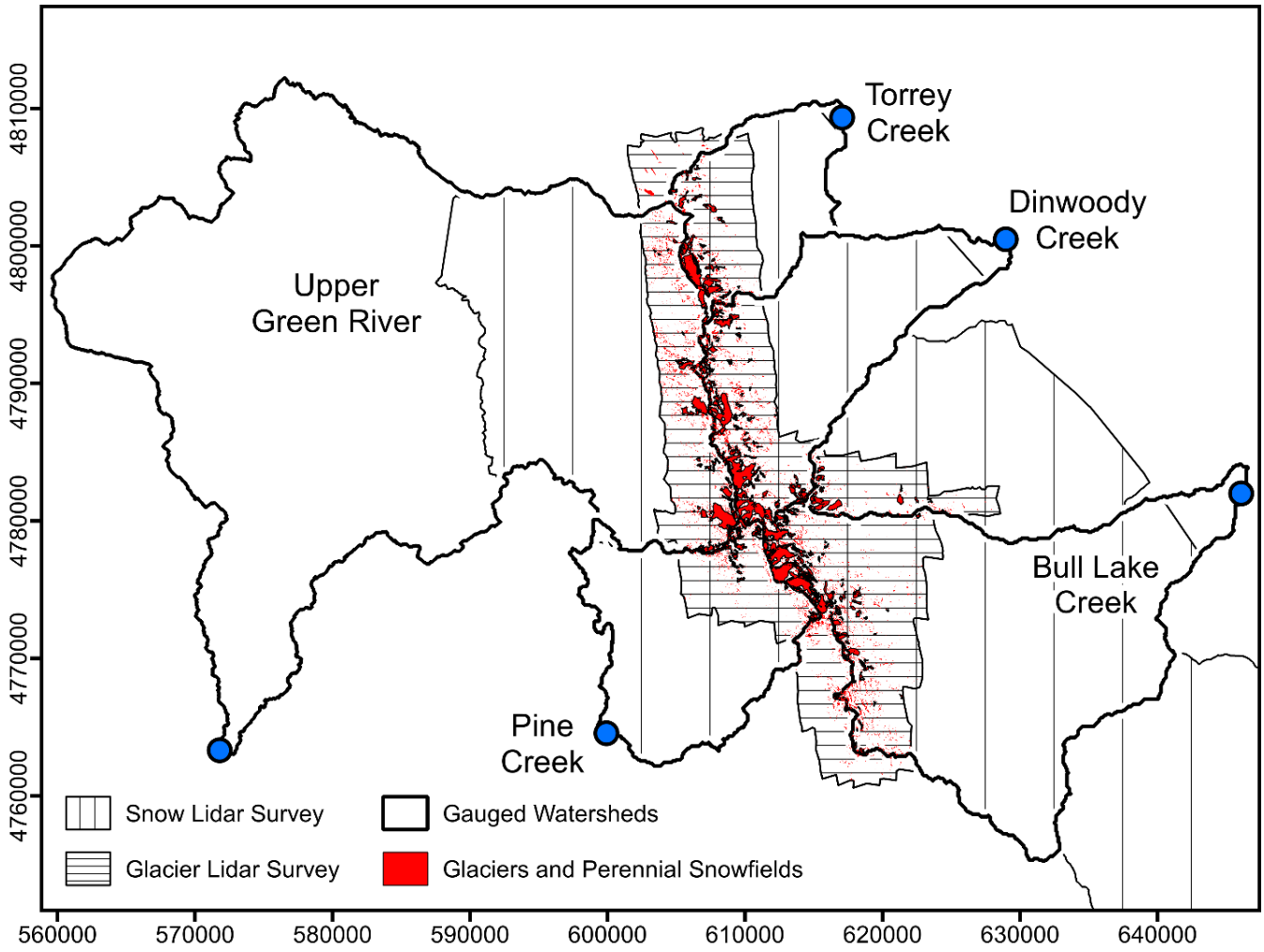

Figure S1: Spatial extent of ASO glacier lidar survey (October 7, 2023) and snow lidar survey (May 31, 2024) relative to the study watersheds and perennial ice and snow features. USGS 3DEP lidar data (August 17-18, 2019) covers the full study region.

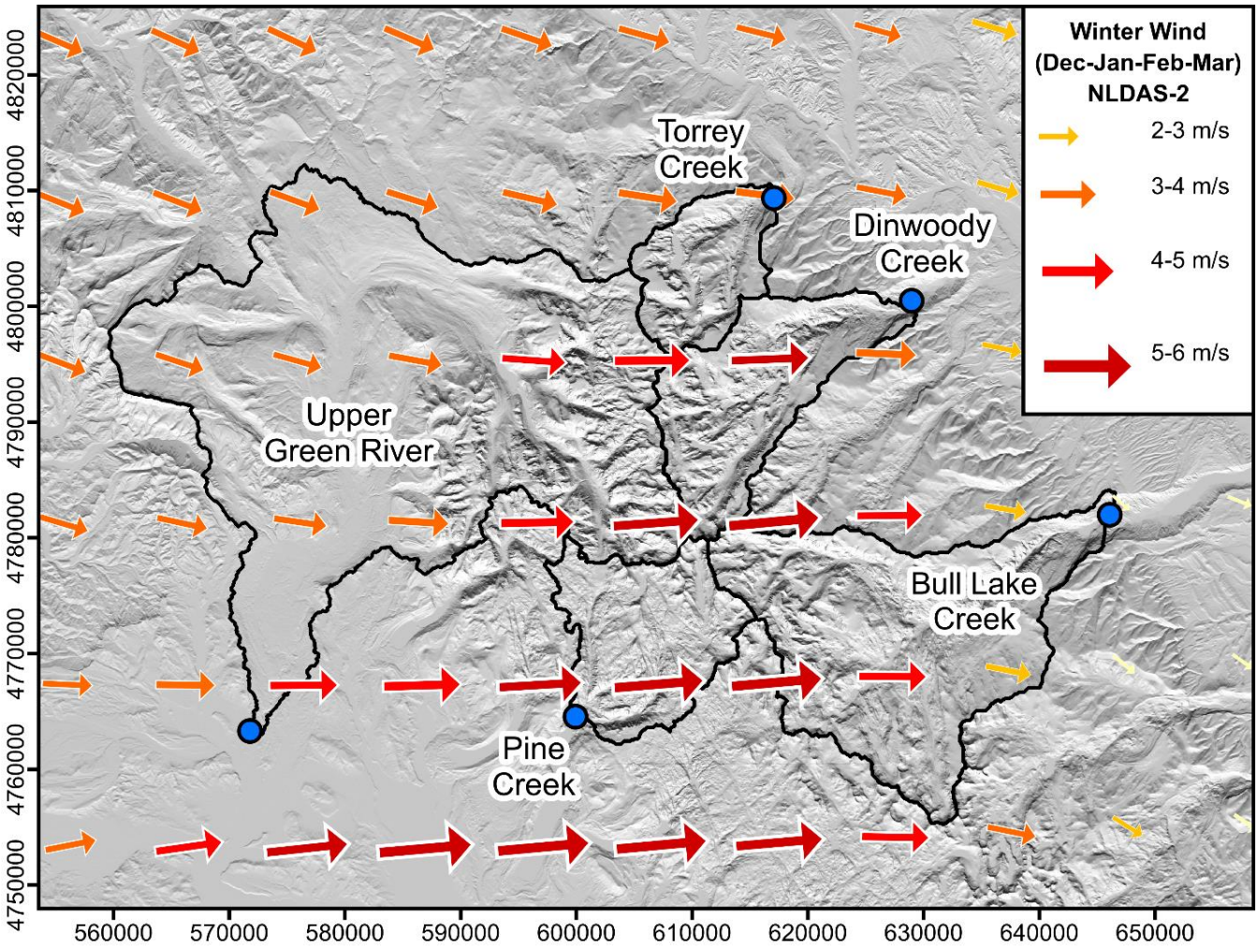

Figure S2: Winter (December through March) mean wind speed and direction from the NLDAS-2 monthly climatology (1980-2009).

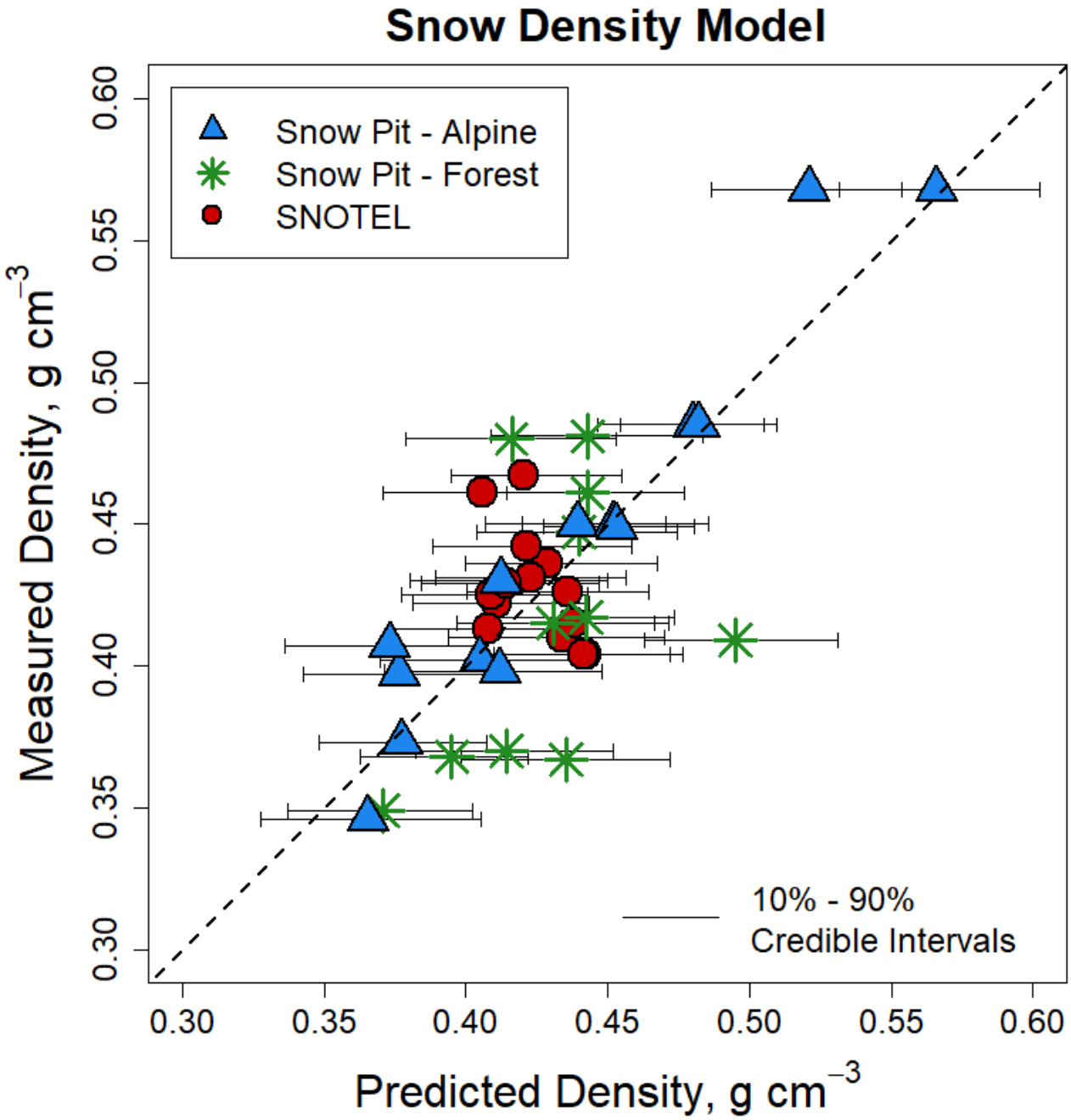

Figure S3: Measured vs. predicted credible intervals for the Bayesian snow density model. Note that the SNOTEL measurements are all below treeline and not representative of alpine snow density variability.

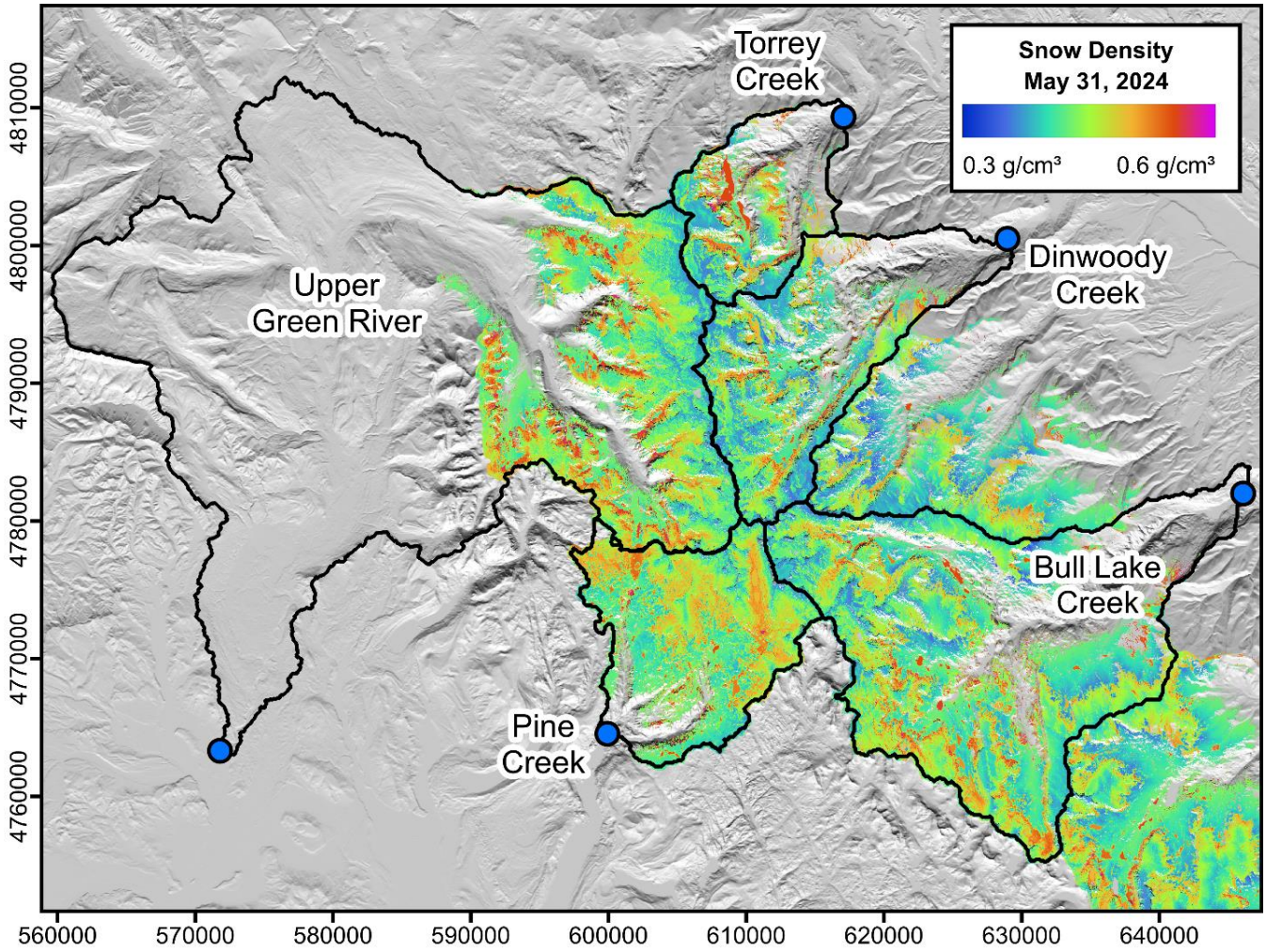

Figure S4: Map of snow density on May 31, 2024, sampled from the Bayesian regression model. Density is only estimated for measured snow depths within the lidar survey area (Fig. S1), and the final SWE depth is imputed outside the survey area (Fig. S5).

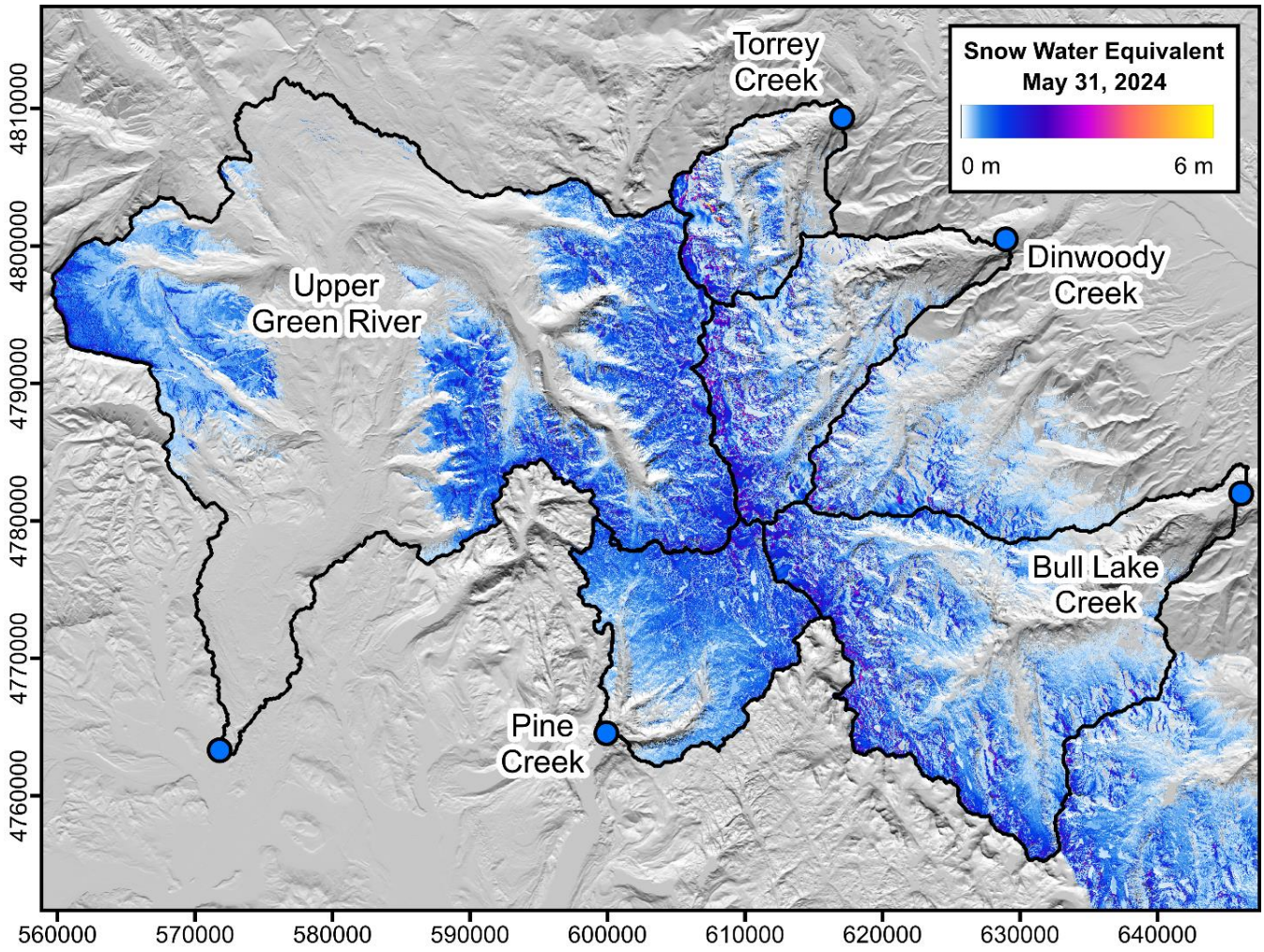

Figure S5: Map of snow water equivalent (SWE) obtained by multiplying the lidar depth map and the density map from Fig. S5. Note that a portion of the Upper Green River watershed beyond the survey extent (Fig. S1) has SWE data imputed by a deep neural network.

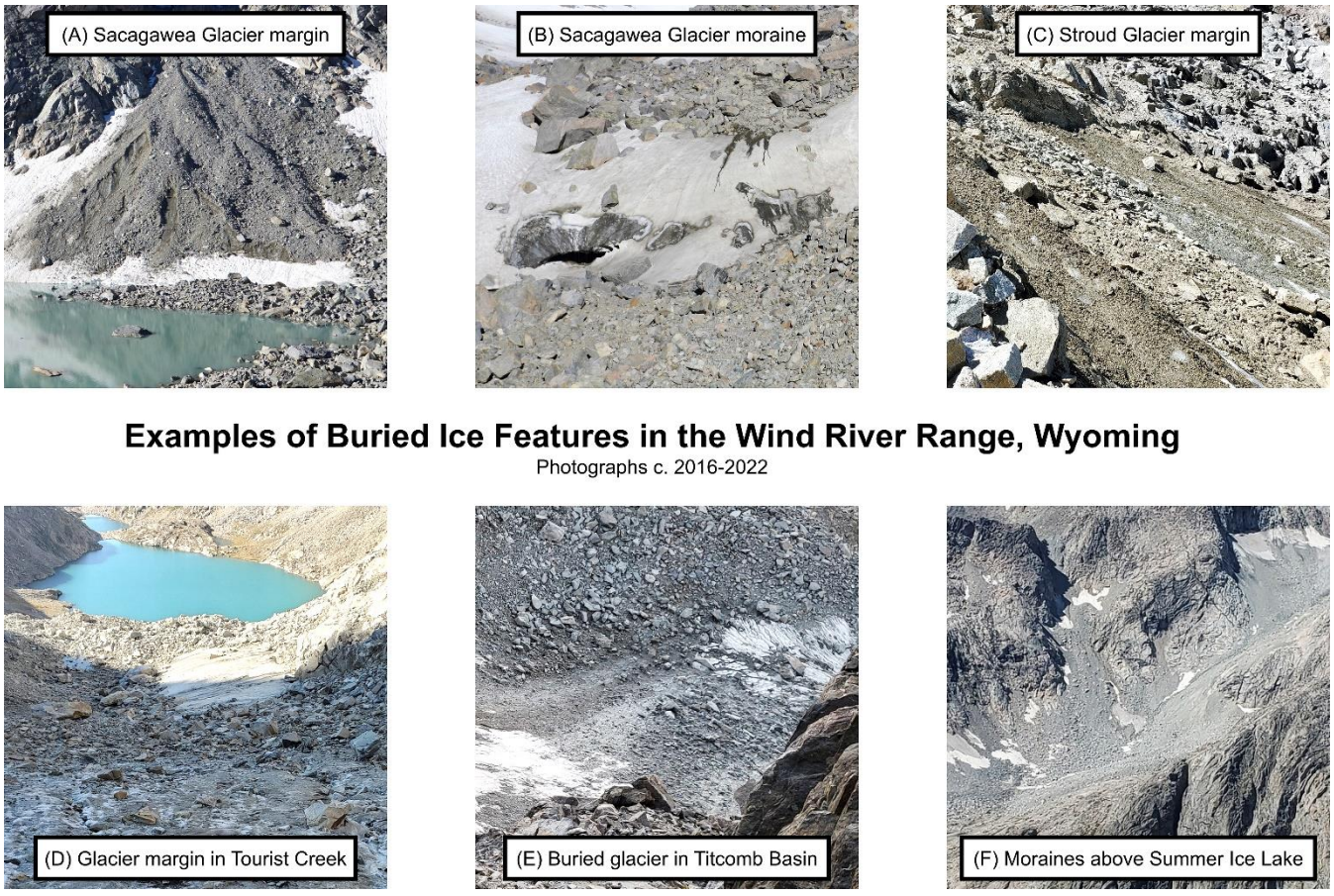

Figure S6: Example photos of buried ice features in the study area, including a variety of debris-mantled glacier margins, ice-cored moraines, and similar features.

30

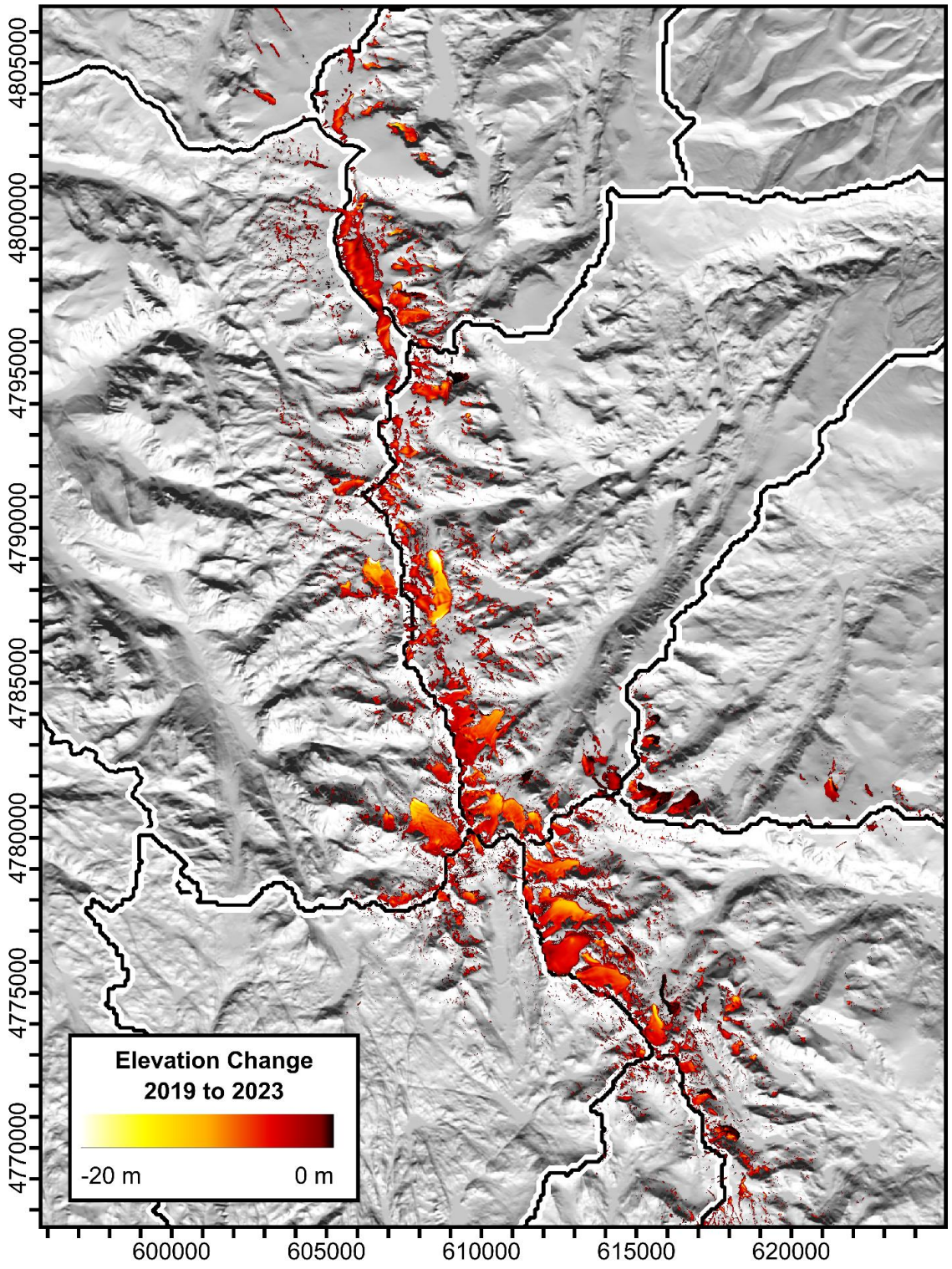

Figure S7: PSI elevation change (not mass) between August 17-18, 2019, and October 7, 2023.

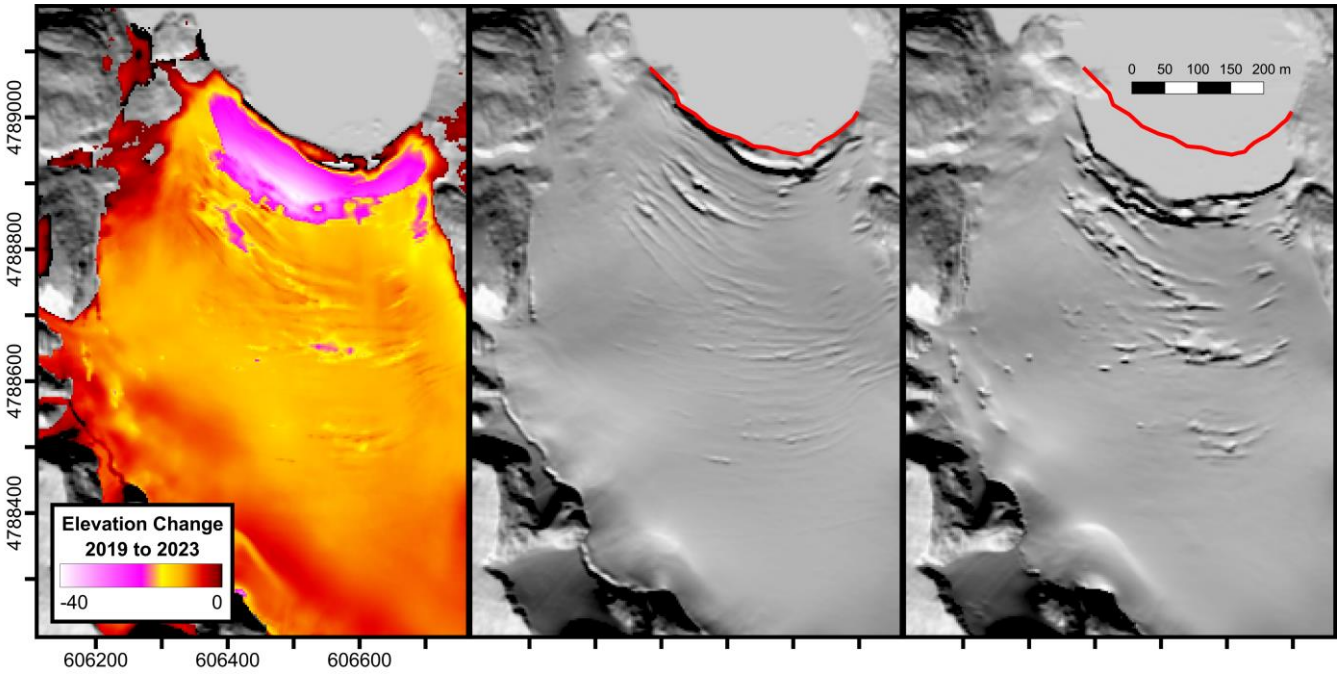

Figure S8: Example of terminal retreat for the Sourdough Glacier. The calving face retreated approximately 60-80 m laterally between 2019 and 2023, with an initial thickness of 20-40 m above the present lake surface.

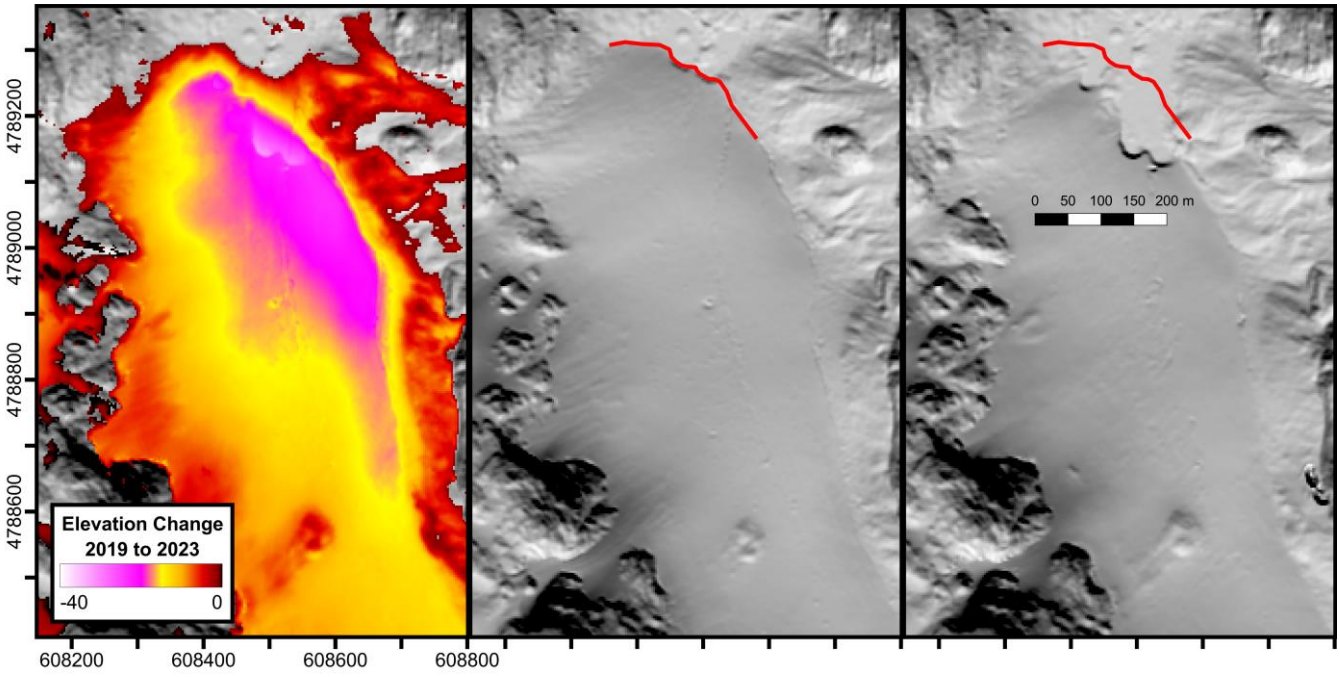

Figure S9: Example of terminal retreat for the Grasshopper Glacier. The terminus retreated approximately 50-120 m, with an initial thickness up to 32 m above the present ground surface.

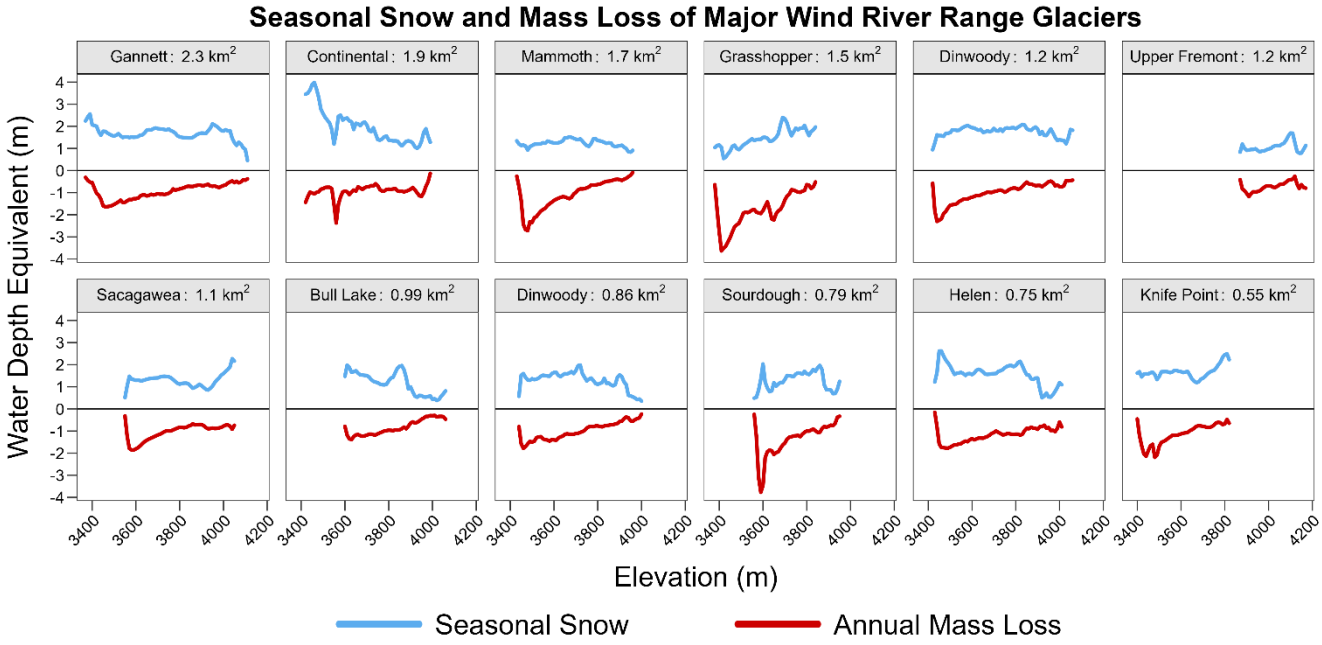

Figure S10: Elevation hypsometry of seasonal snow and annual mass loss for the 12 largest glaciers in the Wind River Range (analogous to Fig. 6 in the main manuscript).

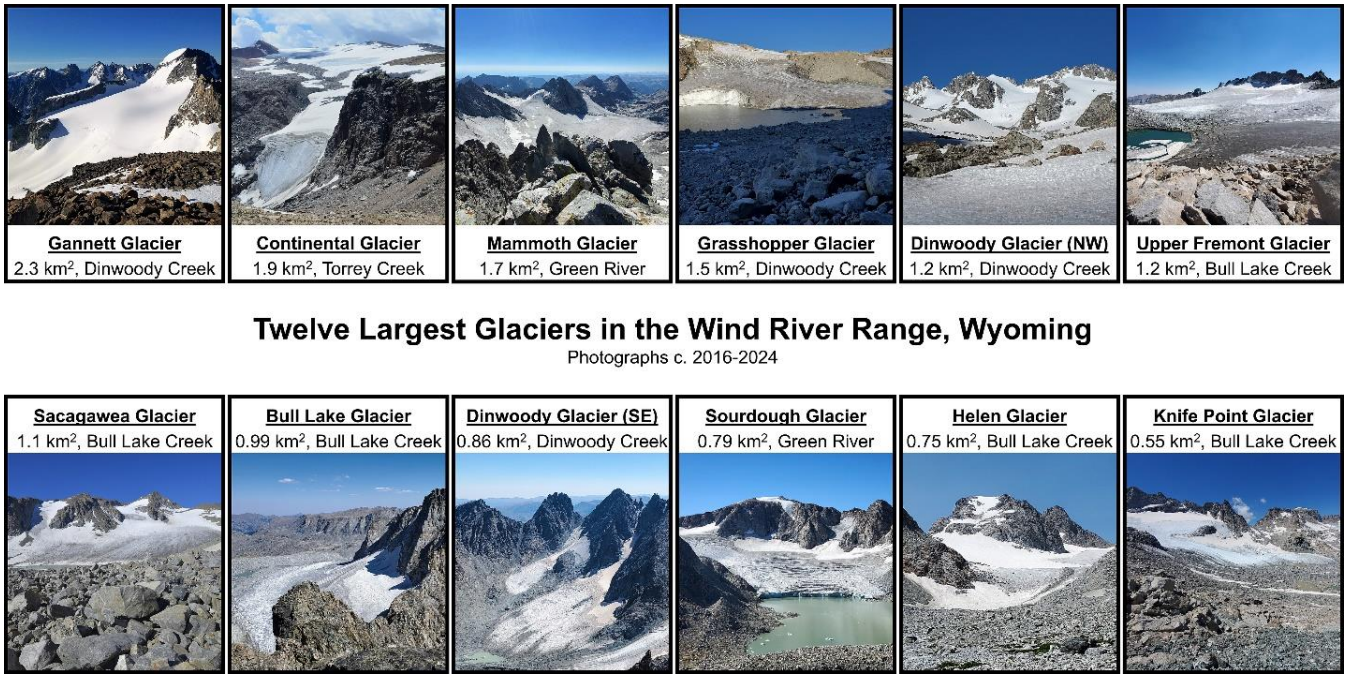

Figure S11: Example photos of the same 12 largest glaciers shown in Fig. S10.

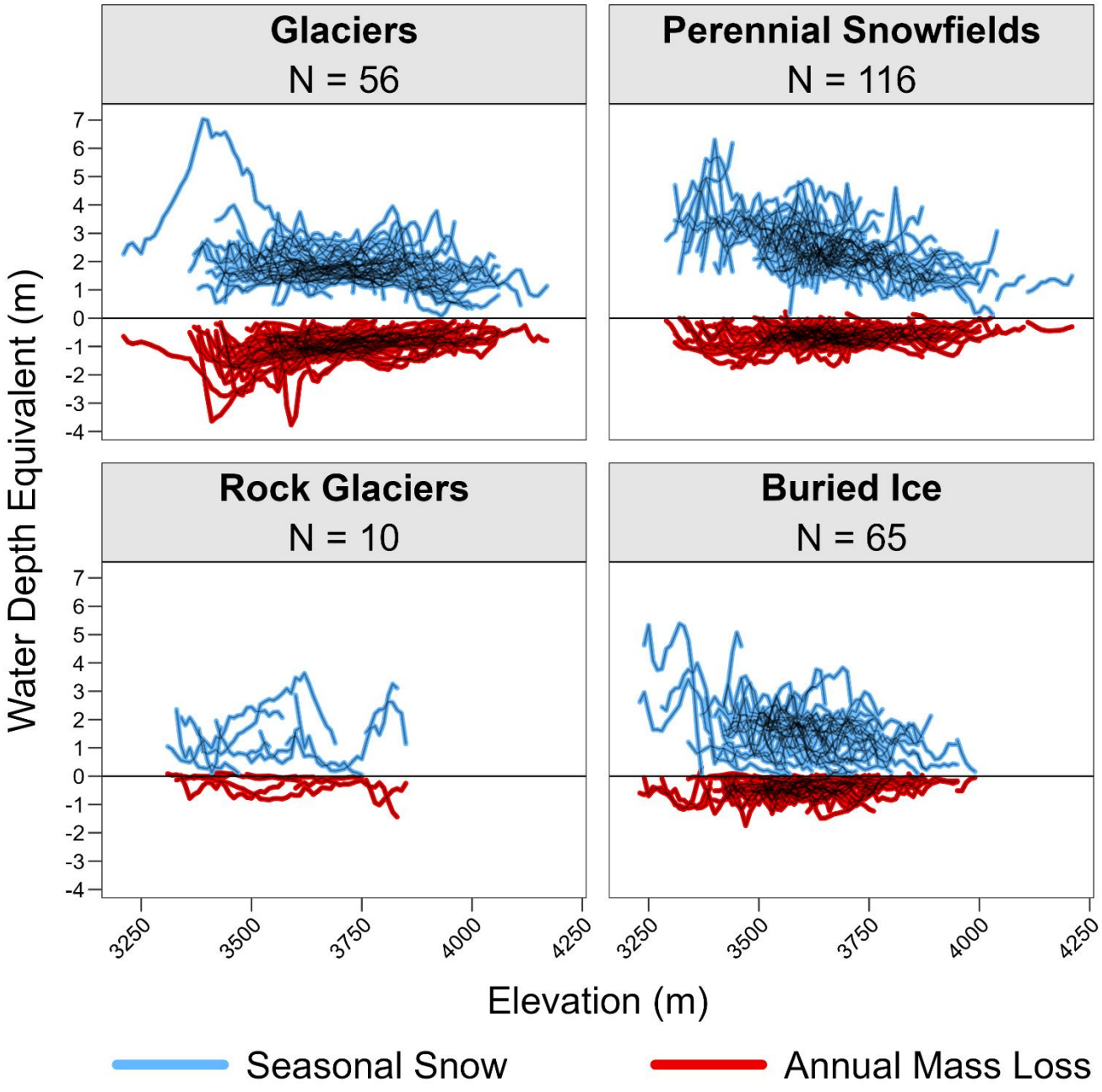

Figure S12: Elevation hypsometry of seasonal snow and annual mass loss for features classified as glaciers, perennial snowfields, rock glaciers, or buried ice (analogous to Figs. 6 and S10).

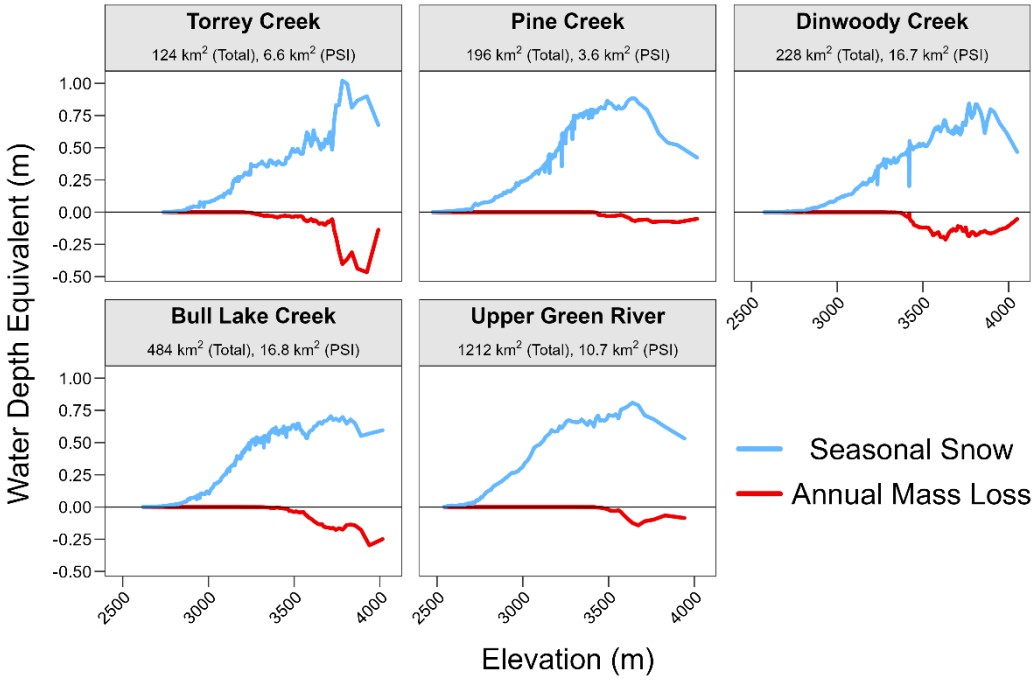

Figure S13: Elevation hypsometry of snow and mass loss by watershed.

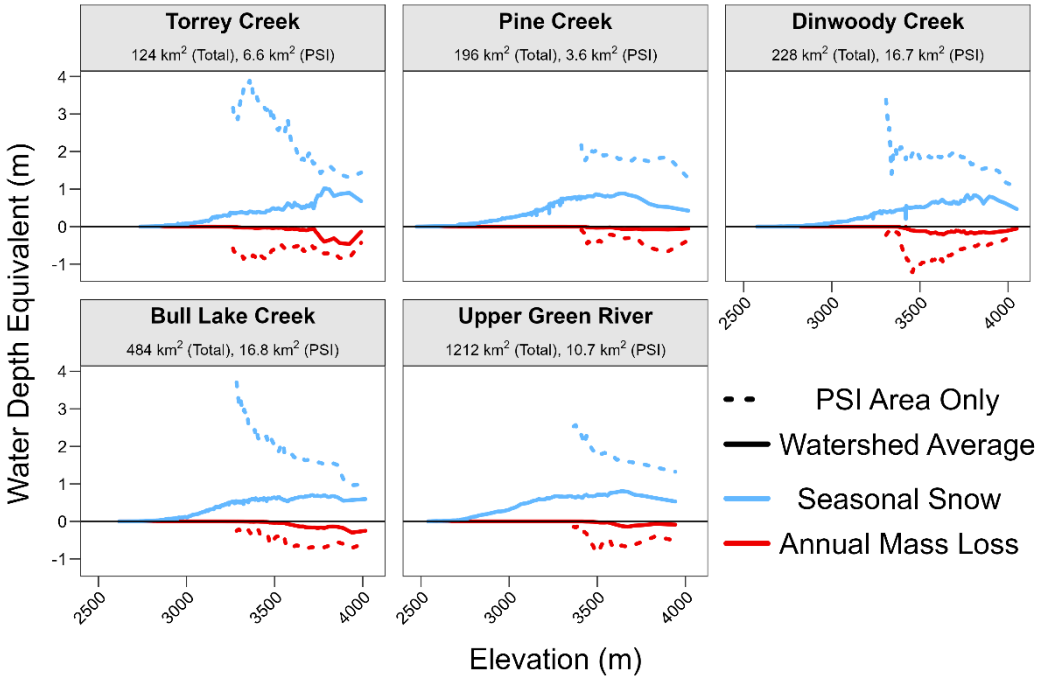

Figure S14: Same as Fig. S13, with the addition of hypsometry curves for the subset of watershed area covered by perennial snow and ice features.

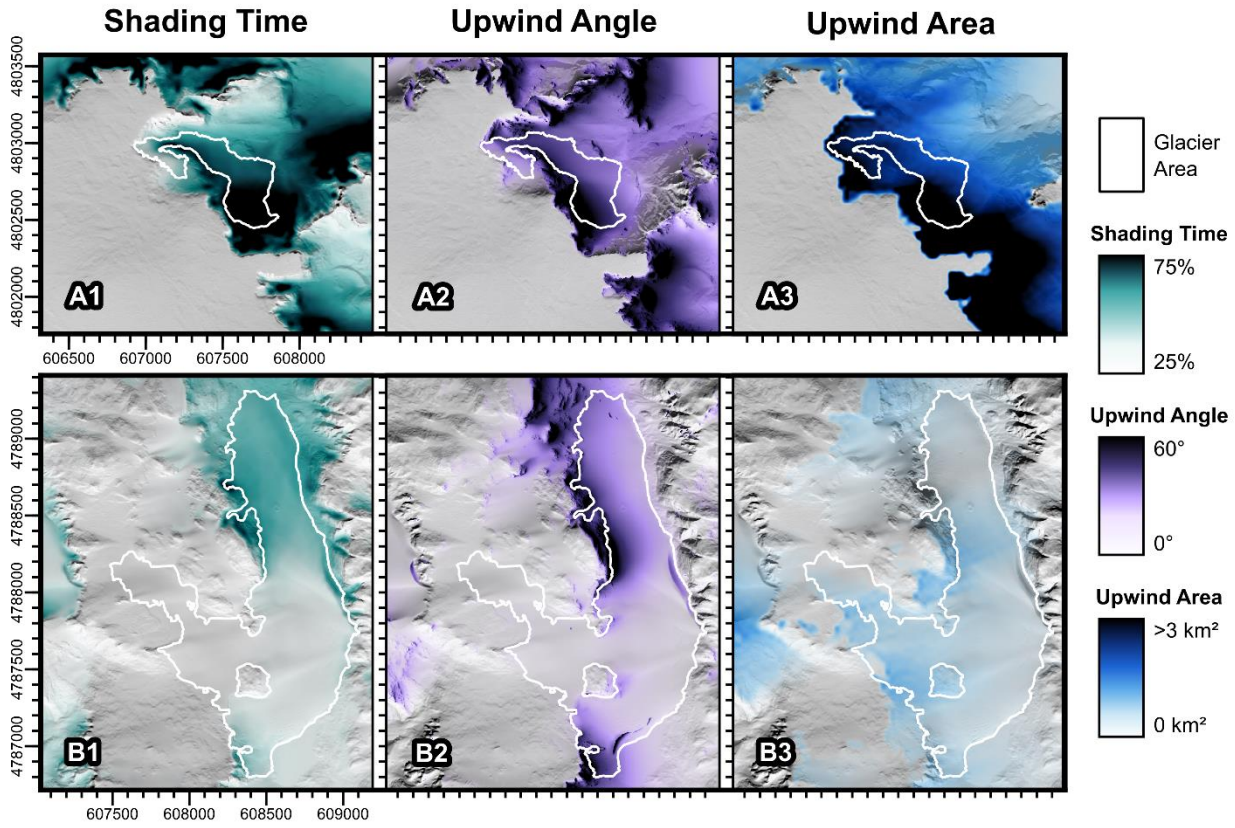

Figure S15: Map of terrain indices for the same glaciers as in Fig. 5 in the main manuscript. Glacier (A) exhibits topographic controls that increase accumulation and limit melt.

Figure S16: Example photos of the two glaciers shown in Figs. 5 and S15: an unnamed glacier c. Ross Lake (A) and the Grasshopper Glacier (B, closer to camera).

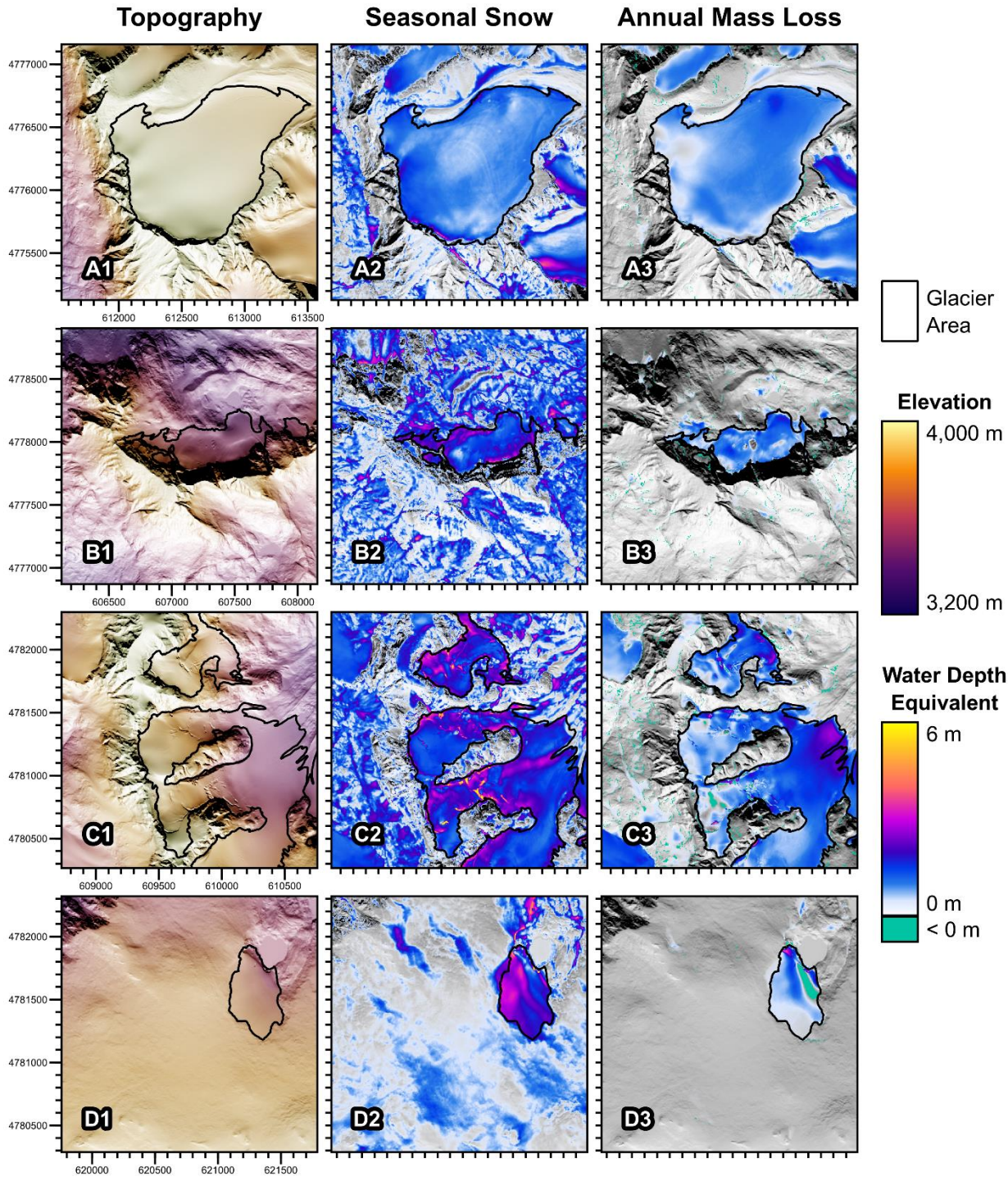

Figure S17: Comparison of seasonal snow and annual mass loss for the four glaciers in Fig. 8 in the main manuscript. Photos of these glaciers are shown in Fig. 4 of the main manuscript.

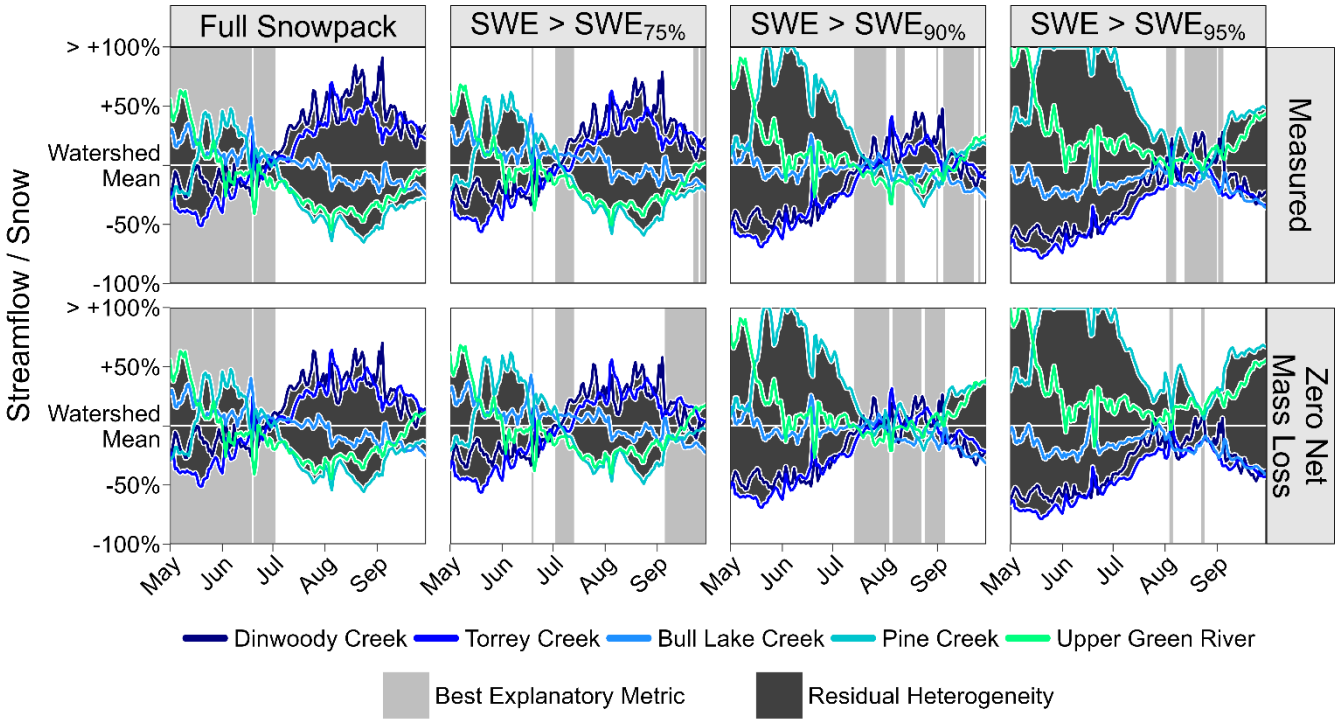

Figure S18: Analogous to Fig. 12 in the main manuscript, but only using water years 2022-2024.